Comput Mech
DOI 10.1007/s00466-013-0869-0

ORIGINAL PAPER

Approximation of incompressible large deformation elastic problems: some unresolved issues

Ferdinando Auricchio · Lourenço Beirão da Veiga · Carlo Lovadina · Alessandro Reali · Robert L. Taylor · Peter Wriggers

Received: 6 December 2012 / Accepted: 2 May 2013

Abstract Several finite element methods for large deformation elastic problems in the nearly incompressible and purely incompressible regimes are considered. In particular, the method ability to accurately capture critical loads for the possible occurrence of bifurcation and limit points, is investigated. By means of a couple of 2D model problems involving a very simple neo-Hookean constitutive law, it is shown that within the framework of displacement/pressure mixed elements, even schemes that are *inf-sup* stable for linear elasticity may exhibit problems when used in the finite deformation regime. The roots of such troubles are identified, but a general strategy to cure them is still missing. Furthermore, a comparison with displacement-based elements, especially of high order, is presented.

Keywords Incompressible nonlinear elasticity · Stability · Mixed finite elements

F. Auricchio · A. Reali
Dipartimento di Ingegneria Civile e Architettura, Università di Pavia, Pavia, Italy
e-mail: alessandro.reali@unipv.it

F. Auricchio · C. Lovadina
Center for Advanced Numerical Simulations—IUSS, Pavia, Italy
e-mail: auricchio@unipv.it

L. Beirão da Veiga
Dipartimento di Matematica, Università di Milano, Milan, Italy
e-mail: lourenco.beirao@unimi.it

C. Lovadina (✉)
Dipartimento di Matematica, Università di Pavia, Pavia, Italy
e-mail: carlo.lovadina@unipv.it

R. L. Taylor
Department of Civil and Environmental Engineering, University of California, Berkeley, CA 94720, USA
e-mail: rlt@ce.berkeley.edu

P. Wriggers
Institute of Continuum Mechanics, Leibnitz University of Hannover, Hannover, Germany
e-mail: wriggers@ikm.uni-hannover.de

1 Introduction

Modern engineering is progressively approaching problems which are always more and more complex, involving phenomena such as strong non-linearities as well as multi-physics and multi-scale phenomena. To do so, the design is often based on the exploitation of sophisticated numerical schemes, developed to reproduce in a virtual computer-based environment such a physical complexity. In particular, designers often tend to use as approximation schemes finite-element methods which are developed, tested and theoretically validated (through standard modern mathematical approaches, e.g., see [12]) for very different situations.

One of the standard realms in which these situations may occur is the case of solid bodies undergoing large deformations and subject to internal material-based constraints, such as volume incompressibility. To solve such non-linear highly constrained problems designers often adopt with "no fear" schemes developed for small-strain regimes.

Accordingly, the goal of the present paper is to show that in some (specific) situations problems may arise and, therefore, caution should be exerted. In particular, at the continuum level finite deformation problems may exhibit physical instabilities, while the corresponding discretizations may exhibit both physical and non-physical (numerical) instabilities, as already identified in previous works (see [27,25,20] and [5]). A fundamental problem is that, due to the lack of closed form

Published online: 18 May 2013

solutions for non-trivial finite-strain problems, it is very difficult to test numerical approximation schemes against the ability to capture only physical stabilities, avoiding instead the raising of numerical non-physical pathological effects. However, we remark that interesting contributions on the finite element approximation of large deformation elasticity problems have been presented also in [11,13,15,26,28] and [29].

The paper is organized as follows. We start focusing on a specific class of materials (i.e., neohookean ones), introduce a Lagrange multiplier approach to properly fulfill the incompressibility constraint at the continuum level and discuss the requirements for a stable continuum response. We then introduce in a formal way possible field discretizations in a Galerkin approach, discussing the requirements for a stable discrete formulation. Finally, we focus the discussion on two specific problems on which we test several different specific approximation schemes, highlighting the raising of some unresolved issues.

2 The large deformation elasticity problem and the stability range

In this paper we adopt the so-called *material description* to study the finite strain elasticity problem (cf., e.g., [10] or [14]). Accordingly, we suppose that we are given a *reference configuration* $\Omega \subset \mathbf{R}^2$ for a bounded material body $\mathcal{B}$. Therefore, the deformation of $\mathcal{B}$ can be described by means of the map $\hat{\varphi} : \Omega \to \mathbf{R}^2$ defined by

$$\hat{\varphi}(\mathbf{X}) = \mathbf{X} + \hat{\mathbf{u}}(\mathbf{X}) , \tag{1}$$

where $\mathbf{X} = (X_1, X_2)$ denotes the coordinates of a material point in the reference configuration and $\hat{\mathbf{u}}(\mathbf{X})$ represents the corresponding displacement vector. Following standard notations (see [10,16,21,22], for instance) we introduce the deformation gradient $\hat{\mathbf{F}} = \mathbf{F}(\hat{\mathbf{u}})$ and the right Cauchy-Green deformation tensor $\hat{\mathbf{C}} = \mathbf{C}(\hat{\mathbf{u}})$ by setting

$$\hat{\mathbf{F}} = \mathbf{I} + \nabla\hat{\mathbf{u}} \quad , \quad \hat{\mathbf{C}} = \hat{\mathbf{F}}^T\hat{\mathbf{F}} , \tag{2}$$

where $\mathbf{I}$ is the second-order identity tensor and ∇ is the gradient operator with respect to the coordinates $\mathbf{X}$.

As usual, we assume that the boundary $\Gamma = \partial\Omega$ is split into two parts, Γ_D and Γ_N, where displacement and traction boundary conditions are respectively imposed. We assume that the measure $\mathrm{meas}(\Gamma_D)$ is strictly positive, in order to neglect rigid body motions. Furthermore, we consider only *homogeneous* displacement boundary conditions. For general displacement boundary conditions, only easy and standard modifications are required. We are interested in external loads whose work is of the form

$$\mathcal{F}(\hat{\mathbf{u}};\gamma) = \gamma\left(\int_\Omega \mathbf{f}\cdot\hat{\mathbf{u}} + \int_{\Gamma_N}\mathbf{p}\cdot\hat{\mathbf{u}}\right) , \tag{3}$$

where γ is a real loading parameter, $\mathbf{f} = \mathbf{f}(\mathbf{X})$ is a given dead bulk load, and $\mathbf{p} = \mathbf{p}(\mathbf{X})$ is a given dead traction. Accordingly, we limit our discussion only to the case of proportional loadings, but this assumption can be easily removed and it does not imply real limitations to the study.

For the description of the large deformation elastic problem we may introduce two possible energy functionals, listed in the following.

– **Displacement-based energy functional** Given a smooth real function $\Theta : \mathbf{R}^+ \to \mathbf{R}$ such that

$$\Theta(J) = 0 \text{ if and only if } J = 1; \tag{4}$$

$$\Theta'(1) \neq 0, \tag{5}$$

and the constant Lamé parameters μ and λ, the elastic energy functional can be written in the following displacement form:

$$\Pi_d(\hat{\mathbf{u}}) = \int_\Omega \left\{\frac{1}{2}\mu\left[\mathbf{I}:\hat{\mathbf{C}}-2\right] - \mu\ln\hat{J} + \frac{\lambda}{2}\Theta(\hat{J})^2\right\} - \mathcal{F}(\hat{\mathbf{u}};\gamma) \tag{6}$$

where $\hat{J} = \det(\hat{\mathbf{F}})$. We remark that $\Theta(\hat{J})$ is the key ingredient to model the elastic energy due to volumetric deformations. Examples of commonly used functions $\Theta(\hat{J})$ are given in Sect. 6.1.1, while details on its physical interpretation can be found in Chap. 7 of [24].

– **Mixed energy functional** Introducing the pressure-like variable $\hat{p} := \lambda\Theta(\hat{J})$ (in the following referred to as *pressure*, for simplicity), the elastic energy functional can be written in the following mixed form:

$$\Pi_m(\hat{\mathbf{u}},\hat{p}) = \int_\Omega \left\{\frac{1}{2}\mu\left[\mathbf{I}:\hat{\mathbf{C}}-2\right] - \mu\ln\hat{J} + \hat{p}\Theta(\hat{J}) - \frac{1}{2\lambda}\hat{p}^2\right\} - \mathcal{F}(\hat{\mathbf{u}};\gamma). \tag{7}$$

In particular, we will be interested in the *purely incompressible case*, which can be obtained by letting $\lambda \to +\infty$ in (7):

$$\Pi_m^{inc}(\hat{\mathbf{u}},\hat{p}) = \int_\Omega \left\{\frac{1}{2}\mu\left[\mathbf{I}:\hat{\mathbf{C}}-2\right] - \mu\ln\hat{J} + \hat{p}\Theta(\hat{J})\right\} - \mathcal{F}(\hat{\mathbf{u}};\gamma). \tag{8}$$

For the displacement-based formulation (6), since pure incompressibility cannot be imposed, we will consider the *nearly incompressible case*, which corresponds to the choice $\lambda >> \mu$.

According to the choices above, we have the corresponding variational formulations described below.

2.1 Displacement-based formulation

In a variational framework, the equilibrium equations stemming from functional (6) are found by imposing $\mathrm{d}\,\Pi_d(\hat{\mathbf{u}})[\mathbf{v}] = 0$ for a generic virtual displacement field $\mathbf{v}$. Explicitly, this reads:

$$\mu \int_\Omega [\hat{\mathbf{F}} - \hat{\mathbf{F}}^{-T}] : \nabla \mathbf{v} \; + \lambda \int_\Omega \Theta(\hat{J})\, \pi(\hat{J})\, \hat{\mathbf{F}}^{-T} : \nabla \mathbf{v} - \mathcal{F}(\mathbf{v}; \gamma) = 0 \tag{9}$$

where the function $\pi(J)$ is defined as

$$\pi(J) = \Theta'(J) J. \tag{10}$$

In studying the stability features of a solution $\hat{\mathbf{u}}$ to Problem (9), a crucial quantity is the second variation of $\Pi_d(\hat{\mathbf{u}})$, i.e. the bilinear form $\mathrm{d}^2\Pi_d(\hat{\mathbf{u}})[\mathbf{u}, \mathbf{v}]$ defined by

$$\begin{aligned} \mathrm{d}^2\Pi_d(\hat{\mathbf{u}})[\mathbf{u}, \mathbf{v}] : = \mu \int_\Omega \nabla \mathbf{u} : \nabla \mathbf{v} + \int_\Omega \left[\mu - \lambda \Theta(\hat{J})\, \pi(\hat{J})\right] \\ \times (\hat{\mathbf{F}}^{-1} \nabla \mathbf{u})^T : \hat{\mathbf{F}}^{-1} \nabla \mathbf{v} + \lambda \int_\Omega \Xi(\hat{J}) \\ \times (\hat{\mathbf{F}}^{-T} : \nabla \mathbf{u})(\hat{\mathbf{F}}^{-T} : \nabla \mathbf{v}) \end{aligned} \tag{11}$$

for every virtual displacement $\mathbf{u}$ and $\mathbf{v}$. In the above, $\Xi(J)$ is defined as

$$\Xi(J) = \Theta(J) \left[\Theta''(J) J^2 + \Theta'(J) J\right] + \pi(J)^2. \tag{12}$$

We introduce the following definition.

Definition 1 A solution $\hat{\mathbf{u}} \in U$ to Problem (9) is a *linearization-stable regular point* if *the coercivity condition* for $\mathrm{d}^2\Pi_d(\hat{\mathbf{u}})$ holds true, i.e.:

$$\alpha_\gamma > 0 \qquad \text{with} \qquad \alpha_\gamma := \inf_{\mathbf{v} \in U} \frac{\mathrm{d}^2\Pi_d(\hat{\mathbf{u}})[\mathbf{v}, \mathbf{v}]}{||\mathbf{v}||_U^2}. \tag{13}$$

In the above, U denotes the space of virtual displacements, equipped with a suitable norm $||\cdot||_U$. For details, refers to [14] or [19].

Remark 1 We remark that assumptions (4) and (5) assure that for an unloaded body (i.e. $\gamma = 0$), the trivial displacement field $\hat{\mathbf{u}} = 0$ is the only solution to the Euler equations (9) and the usual problem is recovered in the infinitesimal elasticity regime. Indeed, a direct computation shows that the corresponding second variation $\mathrm{d}^2\Pi_d(0)[\mathbf{u}, \mathbf{v}]$ (see (11)) reduces to

$$\mathrm{d}^2\Pi_d(0)[\mathbf{u}, \mathbf{v}] := 2\mu \int_\Omega \epsilon(\mathbf{u}) : \epsilon(\mathbf{v}) + \lambda\, \Theta'(1)^2 \int_\Omega \mathrm{div}\mathbf{u}\, \mathrm{div}\mathbf{v}\,, \tag{14}$$

where $\epsilon(\cdot)$ denotes the usual symmetric gradient operator. Therefore, due to Korn's inequality, the bilinear form (14) satisfies the coercivity condition (13) (see [12] or [17], for instance). In addition, we notice that the form (14) is exactly the one involved in classical infinitesimal elasticity problems, with Lamé parameters μ and $\lambda\, \Theta'(1)^2$. This also explains why $\Theta(J)$ is often chosen to satisfy $\Theta'(1) = 1$.

We finally introduce the definition of stability range for Problem (9) .

Definition 2 We define the *stability range* of Problem (9) as the interval $S_d(\mu, \lambda) = (\gamma_m, \gamma_M) \subseteq \mathbf{R}$, where γ_m (resp., γ_M) is the largest negative (resp., smallest positive) value for which the coercivity condition (13) fails.

Therefore, γ_m and γ_M are singular points, such as bifurcation or limit points.

2.2 Mixed formulation (purely incompressible case)

In a variational framework, the equilibrium equations stemming from functional (8) are found by imposing $\mathrm{d}\,\Pi_m^{inc}(\hat{\mathbf{u}})[\mathbf{v}, q] = 0$ for generic virtual displacement and pressure fields $\mathbf{v}$ and q. Explicitly, this reads:

$$\begin{cases} \mu \displaystyle\int_\Omega [\hat{\mathbf{F}} - \hat{\mathbf{F}}^{-T}] : \nabla \mathbf{v} + \int_\Omega \hat{p}\, \pi(\hat{J})\, \hat{\mathbf{F}}^{-T} : \nabla \mathbf{v} - \mathcal{F}(\mathbf{v}; \gamma) = 0 \\ \displaystyle\int_\Omega \Theta(\hat{J})\, q = 0. \end{cases} \tag{15}$$

We remark that the second equation of (15) represents a *nonlinear* constraint.

In studying the stability features of a solution $(\hat{\mathbf{u}}, \hat{p})$ to Problem (15), a crucial quantity is the second variation of $\Pi_m^{inc}(\hat{\mathbf{u}}, \hat{p})$, i.e. the bilinear form $\mathrm{d}^2\Pi_m^{inc}(\hat{\mathbf{u}}, \hat{p})[(\mathbf{u}, p), (\mathbf{v}, q)]$ defined by

$$\mathrm{d}^2\Pi_m^{inc}(\hat{\mathbf{u}}, \hat{p})[(\mathbf{u}, p), (\mathbf{v}, q)] = a_\gamma(\mathbf{u}, \mathbf{v}) + b_\gamma(\mathbf{v}, p) + b_\gamma(\mathbf{u}, q) \tag{16}$$

where

$$\begin{cases} a_\gamma(\mathbf{u}, \mathbf{v}) := \mu \displaystyle\int_\Omega \nabla \mathbf{u} : \nabla \mathbf{v} + \int_\Omega \left[\mu - \hat{p}\, \pi(\hat{J})\right] (\hat{\mathbf{F}}^{-1} \nabla \mathbf{u})^T : \hat{\mathbf{F}}^{-1} \nabla \mathbf{v} \\ \qquad\qquad + \displaystyle\int_\Omega \hat{p}\, \mathsf{k}(\hat{J})\, (\hat{\mathbf{F}}^{-T} : \nabla \mathbf{u})(\hat{\mathbf{F}}^{-T} : \nabla \mathbf{v}) \\ b_\gamma(\mathbf{v}, q) := \displaystyle\int_\Omega q \pi(\hat{J}) \hat{\mathbf{F}}^{-T} : \nabla \mathbf{v}\,, \end{cases} \tag{17}$$

and the function $\mathsf{k}(J)$ is defined as

$$\mathsf{k}(J) = \Theta''(J) J^2 + \Theta'(J) J \tag{18}$$

In addition, $\mathbf{u}$ and $\mathbf{v}$ (p and q) are generic virtual displacement (pressure) fields, respectively. We remark that the forms $a_\gamma(\cdot, \cdot)$ and $b_\gamma(\cdot, \cdot)$ depend on γ, since $\hat{\mathbf{F}}$ and $\hat{p}$ do so.

We now introduce the following definition.

Definition 3 A solution $(\hat{\mathbf{u}}, \hat{p}) \in U \times P$ to Problem (15) $(\hat{\mathbf{u}}, \hat{p}; \gamma)$ is a *linearization-stable regular point* if $\mathrm{d}^2\Pi_d^{inc}(\hat{\mathbf{u}}, \hat{p})$ satisfies *the coercivity on the kernel condition*, i.e. it holds

$$\alpha_\gamma > 0 \qquad \text{with} \qquad \alpha_\gamma := \inf_{\mathbf{v} \in K_\gamma} \frac{a_\gamma(\mathbf{v}, \mathbf{v})}{||\mathbf{v}||_U^2}\,, \tag{19}$$

where

$$K_\gamma := \left\{ \mathbf{v} \in U \;:\; b_\gamma(\mathbf{v}, q) = 0 \qquad \forall q \in P \right\}. \tag{20}$$

In the above, U and P denote the spaces of virtual displacements and virtual pressures, equipped with suitable norms $||\cdot||_U$ and $||\cdot||_P$. For details, refer to [19].

We finally introduce the definition of stability range for Problem (9) .

Definition 4 We define the *stability range* of Problem (9) as the interval $S_m^{inc}(\mu) = (\gamma_m, \gamma_M) \subseteq \mathbf{R}$, where γ_m (resp., γ_M) is the largest negative (resp., smallest positive) value for which the coercivity on the kernel condition (19) fails.

Remark 2 According to Definitions 2 and 4, it can be proved that the stability range computed with the displacement-based formulation letting $\lambda \to +\infty$, coincides with the stability range computed with the purely incompressible mixed formulation, i.e. $\lim_{\lambda\to+\infty} S_d(\mu, \lambda) = S_m^{inc}(\mu)$. The above relation is *independent of the choice of the function* $\Theta(J)$, provided it satisfies conditions (4) and (5) of Remark 1, as detailed in Sect. 2.2.1.

2.2.1 *Independence of the stability range from the choice of* $\Theta(J)$

We now show that the stability range for incompressible materials does not depend on the choice of the function $\Theta(J)$, provided that $\Theta(J)$ satisfies assumptions (4) and (5). We consider a general framework, i.e. we do not restrict to neo-Hookean constitutive laws in 2D, but we here allow for more complicated materials, as well as for different loading histories and possibly for 3D problems. Therefore, we introduce the following functional (cf. (8))

$$\Pi_m^{\Theta}(\hat{\mathbf{u}}, \hat{p}) = \int_\Omega W(\hat{\mathbf{u}}) + \int_\Omega \hat{p}\, \Theta(J(\hat{\mathbf{u}})) - \mathcal{F}(\hat{\mathbf{u}}; \gamma)\,, \tag{21}$$

where $W(\hat{\mathbf{u}})$ is a general elastic energy density function. The equilibrium equations stemming from functional (21) are the equations $\mathrm{d}\,\Pi_m^{\Theta}(\hat{\mathbf{u}}, \hat{p})[\mathbf{v}, q] = 0$ for generic virtual displacement and pressure fields $\mathbf{v}$ and q, i.e. (cf. (15)):

$$\begin{cases} \displaystyle\int_\Omega \mathrm{d}W(\hat{\mathbf{u}})[\mathbf{v}] + \int_\Omega \hat{p}\, \Theta'(J(\hat{\mathbf{u}}))\, \mathrm{d}J(\hat{\mathbf{u}})[\mathbf{v}] - \partial_\gamma \mathcal{F}(\mathbf{v}; \gamma) = 0 \\ \displaystyle\int_\Omega \Theta(J(\hat{\mathbf{u}}))\, q = 0\,, \end{cases} \tag{22}$$

where $\mathrm{d}W(\hat{\mathbf{u}})[\mathbf{v}]$ and $\mathrm{d}J(\hat{\mathbf{u}})[\mathbf{v}]$ denote the variation of $W(\hat{\mathbf{u}})$ and $J(\hat{\mathbf{u}})$ along $\mathbf{v}$, respectively. Also, $\partial_\gamma \mathcal{F}(\mathbf{v}; \gamma)$ is the derivative of $\mathcal{F}(\mathbf{v}; \gamma)$ with respect to γ. We remark, in particular, that the second equation of (22) imposes the constraint $J(\hat{\mathbf{u}}) = 1$.

The second variation of $\Pi_m^{\Theta}(\hat{\mathbf{u}}, \hat{p})$ is defined by (cf. (16) and (17)):

$$\mathrm{d}^2\Pi_m^{\Theta}(\hat{\mathbf{u}}, \hat{p})[(\mathbf{u}, p), (\mathbf{v}, q)] = a_\gamma^{\Theta}(\mathbf{u}, \mathbf{v}) + b_\gamma^{\Theta}(\mathbf{v}, p) + b_\gamma^{\Theta}(\mathbf{u}, q) \tag{23}$$

where

$$\begin{cases} a_\gamma^{\Theta}(\mathbf{u}, \mathbf{v}) := \displaystyle\int_\Omega \mathrm{d}^2 W(\hat{\mathbf{u}})[\mathbf{u}, \mathbf{v}] + \int_\Omega \hat{p}\, \Theta''(J(\hat{\mathbf{u}}))\, \mathrm{d}J(\hat{\mathbf{u}})[\mathbf{u}]\, \mathrm{d}J(\hat{\mathbf{u}})[\mathbf{v}] \\ \qquad\qquad + \displaystyle\int_\Omega \hat{p}\, \Theta'(J(\hat{\mathbf{u}}))\, \mathrm{d}^2 J(\hat{\mathbf{u}})[\mathbf{u}, \mathbf{v}] \\ b_\gamma^{\Theta}(\mathbf{v}, q) := \displaystyle\int_\Omega q \Theta'(J(\hat{\mathbf{u}}))\, \mathrm{d}J(\hat{\mathbf{u}})[\mathbf{v}]. \end{cases} \tag{24}$$

Above, $\mathrm{d}^2 W(\hat{\mathbf{u}})[\mathbf{u}, \mathbf{v}]$ and $\mathrm{d}^2 J(\hat{\mathbf{u}})[\mathbf{u}, \mathbf{v}]$ are, respectively, the second variation of $W(\hat{\mathbf{u}})$ and $J(\hat{\mathbf{u}})$, evaluated for $(\mathbf{u}, \mathbf{v})$.

We now recall that, given $\gamma \in \mathbf{R}$, a solution $(\hat{\mathbf{u}}, \hat{p}) \in U \times P$ to Problem (22) is a *linearization-stable regular point* if $\mathrm{d}^2\Pi_d^{inc}(\hat{\mathbf{u}}, \hat{p})$ satisfies *the coercivity on the kernel condition*, i.e. it holds (cf. Definition 3):

$$\alpha_\gamma := \inf_{\mathbf{v}\in K_\gamma} \frac{a_\gamma^{\Theta}(\mathbf{v}, \mathbf{v})}{||\mathbf{v}||_U^2} > 0\,, \tag{25}$$

where

$$K_\gamma^{\Theta} := \left\{\mathbf{v} \in U \,:\, \Theta'(J(\hat{\mathbf{u}}))\, \mathrm{d}J(\hat{\mathbf{u}})[\mathbf{v}] = 0\right\}. \tag{26}$$

To show that the stability range is independent of the choice of $\Theta(J)$, we fix $\gamma \in \mathbf{R}$ in the stability range (see Definition 4) and a corresponding linearization-stable regular point $(\hat{\mathbf{u}}, \hat{p}) \in U \times P$. We now select a different function $\widetilde{\Theta}(J)$ such that $\widetilde{\Theta}(J) = 0$ if and only if $J = 1$, and $\widetilde{\Theta}'(1) \neq 0$, but holding the same parameter γ fixed. *We want to show that the stability is not affected by this new choice.*

We then consider the couple $(\hat{\mathbf{u}}, \tilde{p})$, where $\tilde{p}$ is defined by

$$\tilde{p} = \hat{p}\frac{\Theta'(1)}{\widetilde{\Theta}'(1)} = \hat{p}\frac{\Theta'(J(\hat{\mathbf{u}}))}{\widetilde{\Theta}'(J(\hat{\mathbf{u}}))}. \tag{27}$$

Since $\Theta(J(\hat{\mathbf{u}})) = \widetilde{\Theta}(J(\hat{\mathbf{u}})) = 0$, from (22) and (27) we infer that the couple $(\hat{\mathbf{u}}, \tilde{p})$ solves

$$\begin{cases} \displaystyle\int_\Omega \mathrm{d}W(\hat{\mathbf{u}})[\mathbf{v}] + \int_\Omega \tilde{p}\, \widetilde{\Theta}'(J(\hat{\mathbf{u}}))\, \mathrm{d}J(\hat{\mathbf{u}})[\mathbf{v}] - \partial_\gamma \mathcal{F}(\mathbf{v}; \gamma) = 0 \\ \displaystyle\int_\Omega \widetilde{\Theta}(J(\hat{\mathbf{u}}))\, q = 0. \end{cases} \tag{28}$$

Therefore, $(\hat{\mathbf{u}}, \tilde{p})$ is a critical point for the functional

$$\Pi_m^{\widetilde{\Theta}}(\hat{\mathbf{u}}, \tilde{p}) = \int_\Omega W(\hat{\mathbf{u}}) + \int_\Omega \tilde{p}\, \widetilde{\Theta}(J(\hat{\mathbf{u}})) - \mathcal{F}(\hat{\mathbf{u}}; \gamma). \tag{29}$$

The second variation of the above functional, evaluated in $(\hat{\mathbf{u}}, \tilde{p})$, reads

$$\mathrm{d}^2\Pi_m^{\widetilde{\Theta}}(\hat{\mathbf{u}}, \tilde{p})[(\mathbf{u}, p), (\mathbf{v}, q)] = a_\gamma^{\widetilde{\Theta}}(\mathbf{u}, \mathbf{v}) + b_\gamma^{\widetilde{\Theta}}(\mathbf{v}, p) + b_\gamma^{\widetilde{\Theta}}(\mathbf{u}, q) \tag{30}$$

where

$$\begin{cases} a_\gamma^{\widetilde{\Theta}}(\mathbf{u}, \mathbf{v}) := \displaystyle\int_\Omega \mathrm{d}^2 W(\hat{\mathbf{u}})[\mathbf{u}, \mathbf{v}] + \int_\Omega \tilde{p}\, \widetilde{\Theta}''(J(\hat{\mathbf{u}}))\, \mathrm{d}J(\hat{\mathbf{u}})[\mathbf{u}]\, \mathrm{d}J(\hat{\mathbf{u}})[\mathbf{v}] \\ \qquad\qquad + \displaystyle\int_\Omega \tilde{p}\, \widetilde{\Theta}'(J(\hat{\mathbf{u}}))\, \mathrm{d}^2 J(\hat{\mathbf{u}})[\mathbf{u}, \mathbf{v}] \\ b_\gamma^{\widetilde{\Theta}}(\mathbf{v}, q) := \displaystyle\int_\Omega q \widetilde{\Theta}'(J(\hat{\mathbf{u}}))\, \mathrm{d}J(\hat{\mathbf{u}})[\mathbf{v}]. \end{cases} \tag{31}$$

Since both $\Theta'(J(\hat{\mathbf{u}})) = \Theta'(1)$ and $\widetilde{\Theta}'(J(\hat{\mathbf{u}})) = \widetilde{\Theta}'(1)$ are different from zero, we deduce (cf. (26))

$$K_\gamma^{\widetilde{\Theta}} = K_\gamma^{\Theta} := \left\{\mathbf{v} \in U \,:\, \mathrm{d}J(\hat{\mathbf{u}})[\mathbf{v}] = 0\right\} := K_\gamma. \tag{32}$$

We now compute $a_\gamma^{\widetilde{\Theta}}(\mathbf{v}, \mathbf{v})$ for a generic $\mathbf{v} \in K_\gamma$. It holds:

$$a_\gamma^{\widetilde{\Theta}}(\mathbf{v}, \mathbf{v}) = \int_\Omega \mathrm{d}^2 W(\hat{\mathbf{u}})[\mathbf{v}, \mathbf{v}] + \int_\Omega \tilde{p}\, \widetilde{\Theta}'(J(\hat{\mathbf{u}}))\, \mathrm{d}^2 J(\hat{\mathbf{u}})[\mathbf{v}, \mathbf{v}]. \tag{33}$$

Recalling (27) and (24), we have

$$a_\gamma^{\widetilde{\Theta}}(\mathbf{v}, \mathbf{v}) = a_\gamma^{\Theta}(\mathbf{v}, \mathbf{v}) \qquad \forall \mathbf{v} \in K_\gamma. \tag{34}$$

Therefore, the *coercivity on the kernel* condition (25) for $a_\gamma^{\Theta}(\cdot, \cdot)$ and for $a_\gamma^{\widetilde{\Theta}}(\cdot, \cdot)$ are equivalent. It follows that

- $(\hat{\mathbf{u}}, \hat{p})$ is a *linearization-stable regular point* for the functional $\Pi_m^{\Theta}(\hat{\mathbf{u}}, \hat{p})$ if and only if $(\hat{\mathbf{u}}, \tilde{p})$ is a *linearization-stable regular point* for the functional $\Pi_m^{\widetilde{\Theta}}(\hat{\mathbf{u}}, \tilde{p})$. As a consequence, the stability range is not affected by the choice of the function $\Theta(J)$.

To summarize, we list below which are the key ingredients to make the stability range independent of $\Theta(J)$.

P1. The non-linear equilibrium equations (22) impose the constraint

$$J(\hat{\mathbf{u}}) = 1 \text{ exactly.} \tag{35}$$

P2. The second variation $\mathrm{d}^2\Pi_m^{\Theta}(\hat{\mathbf{u}}, \hat{p})[(\mathbf{u}, p), (\mathbf{v}, q)]$ (cf. (23) and (32)) has to be tested with virtual displacements $\mathbf{v}$ compatible with the constraint $J(\hat{\mathbf{u}}) = 1$ (i.e. $\mathbf{v} \in K_\gamma$), which explicitly reads:

$$\mathrm{d}J(\hat{\mathbf{u}})[\mathbf{v}] = 0 \text{ exactly.} \tag{36}$$

3 Stability range for the discretized problems via Galerkin approximations

3.1 Stability range for displacement-based approximations

We now introduce a Galerkin approximation of Problem (9) (see, for instance, [4,12,17]). We thus select a finite dimensional subspace $U_h \subset U$ ($h > 0$), and consider the discrete problem

$$\mu \int_\Omega [\hat{\mathbf{F}}_h - \hat{\mathbf{F}}_h^{-T}] : \nabla \mathbf{v}_h + \lambda \int_\Omega \Theta(\hat{J}_h)\, \pi(\hat{J}_h)\, \hat{\mathbf{F}}_h^{-T} : \nabla \mathbf{v}_h - \mathcal{F}(\mathbf{v}_h; \gamma) = 0 \tag{37}$$

for a generic discrete virtual displacement field $\mathbf{v}_h$. In the above, $\hat{\mathbf{F}}_h$ is the discrete deformation gradient corresponding to the unknown discrete displacements $\hat{\mathbf{u}}_h$, and $\hat{J}_h = \det \hat{\mathbf{F}}_h$.

Analogously to what happens for the continuous problem (see Sect. 2.1), the stability for a solution $\hat{\mathbf{u}}_h$ to Problem (37), depends on the second variation of $\Pi_d(\hat{\mathbf{u}}_h)$, i.e. the bilinear form

$$\begin{aligned} \mathrm{d}^2\Pi_d(\hat{\mathbf{u}}_h)[\mathbf{u}_h, \mathbf{v}_h] := {} & \mu \int_\Omega \nabla \mathbf{u}_h : \nabla \mathbf{v}_h \\ & + \int_\Omega \left[\mu - \lambda \Theta(\hat{J}_h)\, \pi(\hat{J}_h)\right] (\hat{\mathbf{F}}_h^{-1} \nabla \mathbf{u}_h)^T : \hat{\mathbf{F}}_h^{-1} \nabla \mathbf{v}_h \\ & + \lambda \int_\Omega \Xi(\hat{J}_h)\, (\hat{\mathbf{F}}_h^{-T} : \nabla \mathbf{u}_h)(\hat{\mathbf{F}}_h^{-T} : \nabla \mathbf{v}_h)\,, \end{aligned} \tag{38}$$

for every virtual discrete displacements $\mathbf{u}_h$ and $\mathbf{v}_h$. We introduce the following definition.

Definition 5 For a solution $\hat{\mathbf{u}}_h \in U_h$ to Problem (37), we say that $(\hat{\mathbf{u}}_h; \gamma)$ is a *linearization-stable regular point* if *the discrete coercivity condition* for $\mathrm{d}^2\Pi_d(\hat{\mathbf{u}}_h)$ holds true, i.e.:

$$\alpha_{\gamma,h} := \inf_{\mathbf{v}_h \in U_h} \frac{\mathrm{d}^2\Pi_d(\hat{\mathbf{u}}_h)[\mathbf{v}_h, \mathbf{v}_h]}{||\mathbf{v}_h||_U^2} > 0. \tag{39}$$

We finally introduce the definition of stability range for Problem (37) .

Definition 6 We define the *stability range* of Problem (37) as the interval $S_{d,h}(\mu, \lambda) = (\gamma_{m,h}, \gamma_{M,h}) \subseteq \mathbf{R}$, where $\gamma_{m,h}$ (resp., $\gamma_{M,h}$) is the largest negative (resp., smallest positive) value for which the coercivity condition (39) fails.

3.2 Stability range for mixed approximations (purely incompressible case)

We now introduce a Galerkin approximation of Problem (15) (see, for instance, [4,12,17]). We thus select a family of finite dimensional subspaces $U_h \subset U$ and $P_h \subset P$ ($h > 0$), and consider the discrete problem

$$\begin{cases} \mu \displaystyle\int_\Omega [\hat{\mathbf{F}}_h - \hat{\mathbf{F}}_h^{-T}] : \nabla \mathbf{v}_h + \int_\Omega \hat{p}_h\, \pi(\hat{J}_h)\, \hat{\mathbf{F}}_h^{-T} : \nabla \mathbf{v}_h - \mathcal{F}(\mathbf{v}_h; \gamma) = 0 \\ \displaystyle\int_\Omega \Theta(\hat{J}_h)\, q_h = 0\,, \end{cases} \tag{40}$$

where $\hat{\mathbf{F}}_h$ is the deformation gradient corresponding to the unknown displacements $\hat{\mathbf{u}}_h$, $\hat{J}_h = \det \hat{\mathbf{F}}_h$ and $\hat{p}_h$ is the discrete unknown pressure field.

Analogously to what happens for the continuous problem (see Sect. 2.2), the stability of a solution $(\hat{\mathbf{u}}_h, \hat{p}_h)$ to Problem (40) depends on the second variation of $\Pi_m^{inc}(\hat{\mathbf{u}}_h, \hat{p}_h)$, i.e. on the bilinear form

$$\begin{aligned} & \mathrm{d}^2\Pi_m^{inc}(\hat{\mathbf{u}}_h, \hat{p}_h)[(\mathbf{u}_h, p_h), (\mathbf{v}_h, q_h)] \\ & \quad = a_{\gamma,h}(\mathbf{u}_h, \mathbf{v}_h) + b_{\gamma,h}(\mathbf{v}_h, p_h) + b_{\gamma,h}(\mathbf{u}_h, q_h) \end{aligned} \tag{41}$$

where

$$\begin{cases} a_{\gamma,h}(\mathbf{u}_h,\mathbf{v}_h) := \mu \displaystyle\int_\Omega \nabla\mathbf{u}_h : \nabla\mathbf{v}_h \\ \qquad\qquad + \displaystyle\int_\Omega \left[\mu - \hat{p}_h\,\pi(\hat{J}_h)\right] (\hat{\mathbf{F}}_h^{-1}\nabla\mathbf{u}_h)^T : \hat{\mathbf{F}}_h^{-1}\nabla\mathbf{v}_h \\ \qquad\qquad + \displaystyle\int_\Omega \hat{p}_h\,\mathsf{k}(\hat{J}_h)\,(\hat{\mathbf{F}}_h^{-T} : \nabla\mathbf{u}_h)(\hat{\mathbf{F}}_h^{-T} : \nabla\mathbf{v}_h) \\ b_{\gamma,h}(\mathbf{v}_h,q_h) := \displaystyle\int_\Omega q_h\pi(\hat{J}_h)\hat{\mathbf{F}}_h^{-T} : \nabla\mathbf{v}_h. \end{cases} \tag{42}$$

We introduce the following definition.

Definition 7 For a solution $(\hat{\mathbf{u}}_h, \hat{p}_h) \in U \times P$ to Problem (40), we say that $(\hat{\mathbf{u}}_h, \hat{p}_h; \gamma)$ is a *linearization-stable regular point* if $\mathrm{d}^2\Pi_d^{inc}(\hat{\mathbf{u}}_h, \hat{p}_h)$ satisfies *the discrete coercivity on the kernel condition*, i.e. it holds

$$\alpha_{\gamma,h} := \inf_{\mathbf{v}\in K_{\gamma,h}} \frac{a_{\gamma,h}(\mathbf{v}_h,\mathbf{v}_h)}{||\mathbf{v}_h||_U^2} > 0 \tag{43}$$

where

$$K_{\gamma,h} := \left\{\mathbf{v}_h \in U_h \;:\; b_{\gamma,h}(\mathbf{v}_h,q_h) = 0 \quad \forall q_h \in P_h\right\}. \tag{44}$$

We finally introduce the definition of stability range for Problem (40) .

Definition 8 We define the *stability range* of Problem (40) as the interval $S_{m,h}^{inc}(\mu) = (\gamma_{m,h}, \gamma_{M,h}) \subseteq \mathbf{R}$, where $\gamma_{m,h}$ (resp., $\gamma_{M,h}$) is the largest negative (resp., smallest positive) value for which the coercivity on the kernel condition (43) fails.

3.3 The influence of the approximation scheme and of $\Theta(J)$ on the stability range

We focus on the mixed formulation for purely incompressible materials (see Sect. 2.2). As shown in Sect. 2.2.1, we first remark that for the continuous problem any smooth choice of $\Theta(J)$ satisfying assumptions (4) and (5) of Remark 1, leads to the same stability range. In our neo-hookean case, the bilinear forms entering in the second variation $\mathrm{d}^2\Pi_m^{inc}(\hat{\mathbf{u}}, \hat{p})[(\mathbf{u}, p), (\mathbf{v}, q)]$ become (see (16) and (17)):

$$\begin{cases} a_\gamma(\mathbf{u},\mathbf{v}) := \mu \displaystyle\int_\Omega \nabla\mathbf{u} : \nabla\mathbf{v} \\ \qquad\qquad + \displaystyle\int_\Omega \left[\mu - \hat{p}\pi(1)\right] (\hat{\mathbf{F}}^{-1}\nabla\mathbf{u})^T : \hat{\mathbf{F}}^{-1}\nabla\mathbf{v} \\ \qquad\qquad + \displaystyle\int_\Omega \hat{p}\,\mathsf{k}(1)\,(\hat{\mathbf{F}}^{-T} : \nabla\mathbf{u})(\hat{\mathbf{F}}^{-T} : \nabla\mathbf{v}) \\ b_\gamma(\mathbf{v},q) := \displaystyle\int_\Omega q\hat{\mathbf{F}}^{-T} : \nabla\mathbf{v}. \end{cases} \tag{45}$$

The key ingredients to make the stability range independent of $\Theta(J)$ are (cf. (35) and (36)) are: *(P1)* the nonlinear equilibrium equations (15) impose the constraint $\hat{J} = 1$ *exactly; (P2)* the second variation $\mathrm{d}^2\Pi_m^{inc}(\hat{\mathbf{u}}, \hat{p})[(\mathbf{u}, p), (\mathbf{v}, q)]$ (cf. (16)) has to be tested with virtual displacements $\mathbf{v}$ compatible with the constraint $\hat{J} = 1$ (i.e. $\mathbf{v} \in K_\gamma$), which here explicitly reads $\hat{\mathbf{F}}^{-T} : \nabla\mathbf{v} = 0$ *exactly*.

In particular, when $\mathbf{v} \in K_\gamma$, we have

$$a_\gamma(\mathbf{v},\mathbf{v}) := \mu \int_\Omega \nabla\mathbf{v} : \nabla\mathbf{v} + \int_\Omega (\mu - \hat{p}\pi(1))\,(\hat{\mathbf{F}}^{-1}\nabla\mathbf{v})^T : \hat{\mathbf{F}}^{-1}\nabla\mathbf{v}. \tag{46}$$

We now consider the discrete problem, i.e. Problem (40). Looking at the second equation, we see that the constraint $\Theta(\hat{J}_h) = 0$ is imposed only *weakly*, through the Lagrange multiplier discrete test functions $q_h \in P_h$.

As a consequence, we do not expect to have, in general, $\hat{J}_h = 1$ *point-wise*. One may argue that, at least for "very fine meshes", the discrete solution should satisfy $\hat{J}_h \approx 1$ (hence $\Theta(\hat{J}_h) \approx 0$ and $\pi(\hat{J}_h) \approx \pi(1) = \Theta'(1)$).

However, even if we assume that the discrete solution is able to enforce $\hat{J}_h = 1$, the forms in the discrete second variation $\mathrm{d}^2\Pi_m^{inc}(\hat{\mathbf{u}}_h, \hat{p}_h)[(\mathbf{u}_h, p_h), (\mathbf{v}_h, q_h)]$ would become (cf. (41) and (42)):

$$\begin{cases} a_{\gamma,h}(\mathbf{u}_h,\mathbf{v}_h) = \mu \displaystyle\int_\Omega \nabla\mathbf{u}_h : \nabla\mathbf{v}_h \\ \qquad\qquad + \displaystyle\int_\Omega \left[\mu - \hat{p}_h\Theta'(1)\right] (\hat{\mathbf{F}}_h^{-1}\nabla\mathbf{u}_h)^T : \hat{\mathbf{F}}_h^{-1}\nabla\mathbf{v}_h \\ \qquad\qquad + \displaystyle\int_\Omega \hat{p}_h\,\left[\Theta''(1) + \Theta'(1)\right]\,(\hat{\mathbf{F}}_h^{-T} : \nabla\mathbf{u}_h) \\ \qquad\qquad\quad \times (\hat{\mathbf{F}}_h^{-T} : \nabla\mathbf{v}_h) \\ b_{\gamma,h}(\mathbf{v}_h,q_h) = \displaystyle\int_\Omega q_h\hat{\mathbf{F}}_h^{-T} : \nabla\mathbf{v}_h\,, \end{cases} \tag{47}$$

where we have used (see (10) and (18))

$$\pi(\hat{J}_h) = \Theta'(1), \quad \mathsf{k}(\hat{J}_h) = \Theta''(1) + \Theta'(1). \tag{48}$$

We are now ready to realize that the discrete stability range is affected by the choice of *(1) the numerical scheme* and of *(2) the function* $\Theta(J)$.

Indeed, we may address the following considerations.

1. *Dependence on the chosen numerical scheme* We notice that, when testing $a_{\gamma,h}(\mathbf{v}_h, \mathbf{v}_h)$ with a generic $\mathbf{v}_h \in K_{\gamma,h}$ (see (44)), the last term of $a_{\gamma,h}(\mathbf{v}_h, \mathbf{v}_h)$ *cannot* be neglected, since $\hat{\mathbf{F}}_h^{-T} : \nabla\mathbf{v}_h$ is *not* zero, in general. Indeed, $\mathbf{v}_h \in K_{\gamma,h}$ means $\hat{\mathbf{F}}_h^{-T} : \nabla\mathbf{v}_h = 0$ only *weakly*. Therefore, the quadratic form to test for the discrete coercivity on the kernel, is

$$\begin{aligned} a_{\gamma,h}(\mathbf{v}_h,\mathbf{v}_h) &= \mu \int_\Omega \nabla\mathbf{v}_h : \nabla\mathbf{v}_h \\ &+ \int_\Omega \left[\mu - \hat{p}_h\Theta'(1)\right] (\hat{\mathbf{F}}_h^{-1}\nabla\mathbf{v}_h)^T : \hat{\mathbf{F}}_h^{-1}\nabla\mathbf{v}_h \\ &+ \int_\Omega \hat{p}_h\,\left[\Theta''(1) + \Theta'(1)\right]\,(\hat{\mathbf{F}}_h^{-T} : \nabla\mathbf{v}_h)(\hat{\mathbf{F}}_h^{-T} : \nabla\mathbf{v}_h). \end{aligned} \tag{49}$$

We remark that the first two terms in (49) are consistent, up to the approximation of $(\hat{\mathbf{u}}, \hat{p})$ by means of $(\hat{\mathbf{u}}_h, \hat{p}_h)$, with the corresponding ones at the continuous level (cf. (46)). However, since the two terms above have to be tested for $\mathbf{v}_h \in K_{\gamma,h}$, which does not imply $\hat{\mathbf{F}}_h^{-T} : \nabla \mathbf{v}_h = 0$, the positivity of the form

$$\mu \int_\Omega \nabla \mathbf{v}_h : \nabla \mathbf{v}_h + \int_\Omega \left[\mu - \hat{p}_h \Theta'(1)\right] (\hat{\mathbf{F}}_h^{-1} \nabla \mathbf{v}_h)^T : \hat{\mathbf{F}}_h^{-1} \nabla \mathbf{v}_h$$

does depend on the selected numerical scheme, since $K_{\gamma,h}$ does so. In particular, we expect that:

- *the more $K_{\gamma,h}$ is "close" to the continuous kernel K_γ* (cf. (20)), *the more the discrete stability range will be well-approximated by the numerical method.*

2. *Dependence on the chosen function $\Theta(J)$* We see that the term

$$\int_\Omega \hat{p}_h \left[\Theta''(1) + \Theta'(1)\right] (\hat{\mathbf{F}}_h^{-T} : \nabla \mathbf{v}_h)(\hat{\mathbf{F}}_h^{-T} : \nabla \mathbf{v}_h) \tag{50}$$

represents a potential source of *stability* or *instability* for the discrete problem, depending on the product $\hat{p}_h\,[\Theta''(1) + \Theta'(1)]$. In any case, we expect that the discrete stability range $S^{inc}_{m,h}(\mu)$ may depend on the choice of $\Theta(J)$ through its derivatives $\Theta'(1)$ and $\Theta''(1)$ (and especially through the sign of $[\Theta''(1) + \Theta'(1)]$.

Remark 3 We remark that the troubles cannot be avoided by simply insisting that $[\Theta''(1)+\Theta'(1)] = 0$. Indeed, this choice only results in making the term (50) negligible. However, the problems arising from the choice of the numerical scheme still needs to be solved. We will see in Sect. 6 that $\Theta(J) = \ln J$, which satisfies $[\Theta''(1)+\Theta'(1)] = 0$, is not a satisfactory choice, in general.

To summarize all the previous discussion, we list below the two main sources that make the satisfaction of the discrete *coercivity on the kernel* condition (7) possibly dependent on the choice of $\Theta(J)$ and on the approximation scheme, *thus potentially spoiling the good approximation of the stability range.*

S1$_h$. The non-linear equilibrium equations (40) impose the constraint

$$\hat{J}_h = 1 \text{ only weakly.} \tag{51}$$

S2$_h$. The second variation $\mathrm{d}^2\Pi^{inc}_m(\hat{\mathbf{u}}_h, \hat{p}_h)[(\mathbf{u}_h, p_h), (\mathbf{v}_h, q_h)]$ (cf. (41)) has to be tested with virtual displacements $\mathbf{v}_h$ belonging to the discrete kernel $K_{\gamma,h}$, thus satisfying

$$\hat{\mathbf{F}}_h^{-T} : \nabla \mathbf{v}_h = 0 \text{ only weakly.} \tag{52}$$

We remark that Property (52) means *relaxing* the linearized incompressibility constraint, a strategy commonly used to avoid the *volumetric locking phenomenon* in mixed finite element schemes, especially of low-order. Therefore, we expect that:

- if the constraint $\hat{J}_h = 1$ is imposed *too weakly*, one risks a failure in efficiently detecting the stability range of the problem under consideration;
- if the constraint $\hat{J}_h = 1$ is imposed *almost exactly*, one risks volumetric locking phenomenon to occur.

To the best authors' knowledge, a rigorous theory concerning a "correct balancing" for the incompressibility constraint imposition, or general cures for "unbalanced" schemes, is still missing in this context.

4 Two examples

We now present two problems which are then used as benchmarks in Sect. 6 to explore the performance of the numerical schemes under investigation (and presented in Sect. 5) in approximating the stability range. However, we point out that, since no rigorous general theory on the stability range approximation is available, numerical schemes passing these benchmarks, are not necessarily reliable for a generic large deformation elastic problem.

4.1 Problem 1

This problem has already been considered in [5] and [6], but only with a specific choice of the volumetric term modeling (i.e., with a specific choice of $\Theta(J)$). We consider a square material body with reference configuration $\Omega = (-1, 1) \times (-1, 1)$, as shown in Fig. 1.

The upper part of the body boundary is traction free, while the remaining boundary is clamped. The body is subjected to a vertical uniform body force $\gamma\mathbf{f}$ with $\mathbf{f} = (0, 1)^T$ and γ a real loading parameter (cf. (3)).

Reference [5] reported that for every $\gamma \in \mathbf{R}$ the problem admit at least a trivial solution, i.e. $\widehat{\mathbf{u}} = \mathbf{0}$ and $\widehat{p} = \gamma(1 - Y)$. It is also proved that for this problem the stability range (cf. Definition 4) is

$$S^{inc}_m(\mu) = (-\infty, \gamma_M), \tag{53}$$

with γ_M a suitable positive real number. In Reference [6] a very accurate estimate $\gamma_M \approx 6.6\,\mu$ has been computed, by means of NURBS approximation schemes (see [8] and [18], for instance), based on a suitable *stream function formulation*

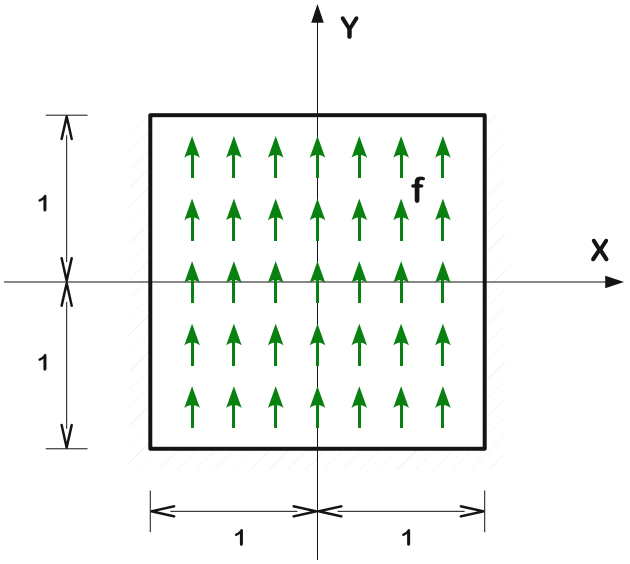

Fig. 1 Problem 1.

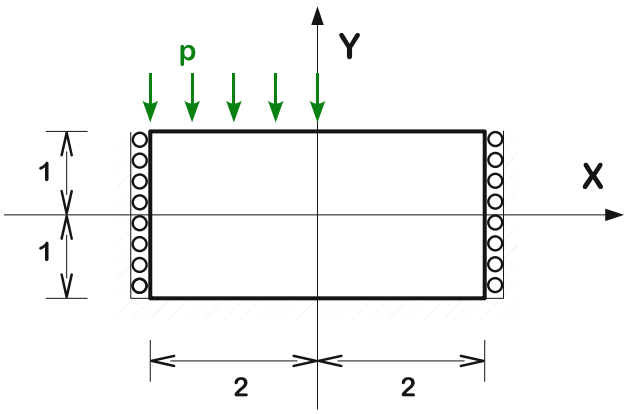

Fig. 2 Problem 2.

of the linearized problem. Therefore, in the following we will consider $\gamma_M = 6.6\,\mu$ as the optimal target value for the numerical schemes in detecting the supremum of the problem stability range.

4.2 Problem 2

We consider a rectangular material body with reference configuration $\Omega = (-2, 2) \times (-1, 1)$, as shown in Fig. 2.

The bottom part of the body boundary is clamped, while both left and right sides are on vertical rollers, hence constraining only the horizontal displacements. Finally, the left top part of the body is subjected to a vertical uniform load per unit length, while the right top part is set to be traction free.

The surface uniform load can be expressed as $\gamma \mathbf{p}$ with $\mathbf{p} = (0, -1)^T$ and γ a real loading parameter (cf. (3)).

Trivial solutions to the problem are not available, for $\gamma \neq 0$. In addition, as far as we know, for this problem nothing is known concerning the stability range, neither theoretically nor computationally.

5 Numerical schemes

We now introduce the finite element schemes we used for the analyses of the problems detailed in Sect. 4. Let $\mathcal{T}_h$ be a triangular or a quadrilateral mesh of Ω, h being the meshsize. In the sequel, we denote with $P_k(K)$ the space of polynomial functions of degree at most k, defined on the generic element K. Also, for a generic quadrilateral element K, $Q_k(K)$ denotes the space of polynomial functions of degree at most k with respect to each variable ξ and η, where (ξ, η) are the standard local coordinates on K.

5.1 Displacement-based finite element methods

Concerning formulation (37), we have considered the following elements (see, e.g., [12,17]).

– **The Tk elements** For triangular meshes and for $4 \geq k \geq 2$, we set the discrete displacement space as

$$U_h = \left\{ \mathbf{v}_h \in U \cap C^0(\Omega)^2 \ : \ \mathbf{v}_{h|T} \in P_k(T)^2 \qquad \forall T \in \mathcal{T}_h \right\}. \tag{54}$$

Therefore, the displacements are approximated by means of continuous functions. We remark that here we do not consider the case $k = 1$, because that choice leads to the most severe volumetric locking phenomenon.

5.2 Mixed finite element methods

Concerning formulation (40), we have considered the following elements.

– **The MINI element** (see [3] or [12], for instance). It is a triangular element. For the discretization of the displacement field, we take

$$U_h = \left\{ \mathbf{v}_h \in U \cap C^0(\Omega)^2 \ : \ \mathbf{v}_{h|T} \in P_1(T)^2 + B(T)^2 \qquad \forall T \in \mathcal{T}_h \right\}, \tag{55}$$

where $B(T)$ is the linear space generated by b_T, the standard cubic bubble function on T. For the pressure discretization, we take

$$P_h = \left\{ q_h \in C^0(\Omega) \ : \ q_{h|T} \in P_1(T) \quad \forall T \in \mathcal{T}_h \right\}. \tag{56}$$

Therefore, both the displacements and the pressures are approximated by means of continuous functions. This element is well known to be stable in the incompressible range in linear elasticity.

– **The Qk/P$(k-1)$ element** (see [12] or [17], for instance). For $k = 1, 2$, they are classical quadrilateral elements. For the discretization of the displacement field, we take

$$U_h = \left\{ \mathbf{v}_h \in U \cap C^0(\Omega)^2 \ : \ \mathbf{v}_{h|K} \in Q_k(K)^2 \quad \forall K \in \mathcal{T}_h \right\}. \tag{57}$$

For the pressure discretization, we take

$$P_h = \left\{ q_h \in P \ : \ q_{h|K} \in P_{k-1}(K) \quad \forall K \in \mathcal{T}_h \right\}. \tag{58}$$

Therefore, the displacements and the pressures are approximated by means of continuous and discontinuous functions, respectively. For $k = 2$, the element is well known to be stable in the incompressible range in linear elasticity.

– **The Tk/T$(k-1)$ elements (Taylor-Hood elements)** (see [12] or [17], for instance). They are triangular elements with continuous pressure approximation. Fix $k \geq 2$. For the discretization of the displacement field, we take

$$U_h = \left\{ \mathbf{v}_h \in U \cap C^0(\Omega)^2 \ : \ \mathbf{v}_{h|T} \in P_k(T)^2 \quad \forall T \in \mathcal{T}_h \right\}. \tag{59}$$

For the pressure discretization, we take

$$P_h = \left\{ q_h \in C^0(\Omega) \ : \ q_{h|T} \in P_{k-1}(T) \quad \forall T \in \mathcal{T}_h \right\}. \tag{60}$$

Therefore, both the displacements and the pressures are approximated by means of continuous functions. Under minor restrictions on the used meshes, these elements are stable in the incompressible range in linear elasticity.

– **The T2/P0 element** (see [4] or [12], for instance) It is a triangular element. For the discretization of the displacement field, we take

$$U_h = \left\{ \mathbf{v}_h \in U \cap C^0(\Omega)^2 \ : \ \mathbf{v}_{h|T} \in P_2(T)^2 \quad \forall T \in \mathcal{T}_h \right\}. \tag{61}$$

For the pressure discretization, we take

$$P_h = \left\{ q_h \in P \ : \ q_{h|T} \in P_0(T) \quad \forall T \in \mathcal{T}_h \right\}. \tag{62}$$

Therefore, the displacements and the pressures are approximated by means of continuous and discontinuous functions, respectively. This element is well known to be stable in the incompressible range in linear elasticity.

6 Numerical results

We now report the numerical results relative to the approximation of the stability range for the two problems detailed in Sect. 4 using the schemes addressed in Sect. 5.

Both problems are studied with different square meshes, indicated as $n \times m$, with n and m referring to the number of subdivisions in direction x and y, respectively. Obviously, for Problem 1 of Sect. 4.1 we have $n = m$, while for Problem 2 of Sect. 4.2 we have $n = 2m$. When triangular elements are employed, the meshes are obtained by dividing each square element by means of one diagonal (see Fig. 3)

All the methods are implemented through the code AceGen © and the problems are solved using AceFEM© and adopting a Newton iteration solver. For details on AceGen© and AceFEM© see [2] and [1], respectively.

We consider the following value for the material constants

$$\mu = 40\,, \ \lambda = 10^5 \mu.$$

We remark that the value of λ is used only for the displacement-based formulations and it is set to reproduce an almost incompressible situation.

For both problems and all analyses, we start from the unloaded state and we progressively increase the load until the first *numerical critical value* is found. The *numerical critical value* is here defined as the point where a sign change for the tangent matrix eigenvalues occurs. It can be proved that this actually means that the *numerical critical value* is essentially the first value when:

– for displacement-based schemes, the *discrete coercivity condition* (39) fails;
– for mixed schemes, the *discrete coercivity on the kernel condition* (43) fails.

All the results are reported using the scaled loading parameter $\bar{\gamma} = \frac{\gamma}{\mu}$, and the computed critical values are denoted as $\bar{\gamma}_{cr}$.

6.1 Numerical results for Problem 1 (Sect. 4.1)

6.1.1 Tension test

For this problem, we explore the numerical capability in detecting the correct stability range for all the numerical schemes introduced in Sect. 5. In addition, for every scheme

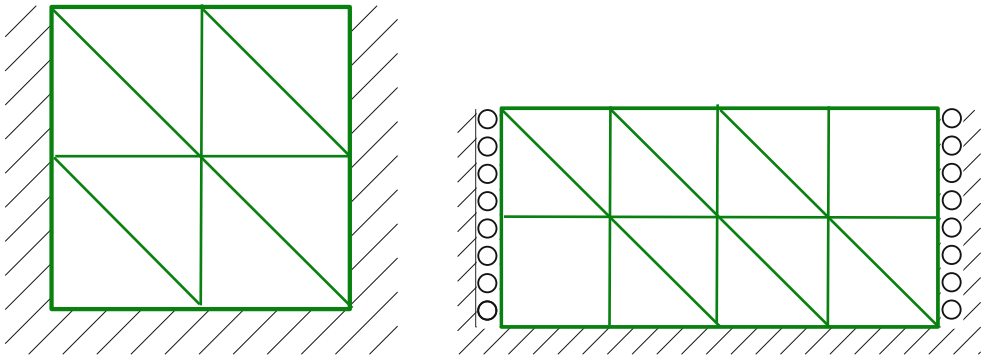

Fig. 3 Typical triangular mesh for Problem 1 (*left*), and for Problem 2 (*right*).

Table 1 Problem 1—Results for different functions $\Theta(J)$, displacement-based elements

Elm	$\Theta(J)$	Mesh	$\bar{\gamma}_{cr}$ tension	Elm	$\Theta(J)$	Mesh	$\bar{\gamma}_{cr}$ tension
T4	$(J-1)$	4×4	6.67	T2	$(J-1)$	8×8	6.90
		8×8	6.62			16×16	6.68
		16×16	6.60			32×32	6.63
		32×32	6.60			64×64	6.63
	$\log J$	4×4	6.67		$\log J$	8×8	6.90
		8×8	6.62			16×16	6.69
		16×16	6.60			32×32	6.63
		32×32	6.60			64×64	6.63
	$(1-\frac{1}{J})$	4×4	6.67		$(1-\frac{1}{J})$	8×8	6.90
		8×8	6.62			16×16	6.68
		16×16	6.60			32×32	6.62
		32×32	6.60			64×64	6.60
T3	$(J-1)$	8×8	6.64				
		16×16	6.61				
		32×32	6.60				
		64×64	6.60				
	$\log J$	8×8	6.64				
		16×16	6.62				
		32×32	6.60				
		64×64	6.60				
	$(1-\frac{1}{J})$	8×8	6.64				
		16×16	6.61				
		32×32	6.60				
		64×64	6.60				

and every mesh, we select three different choices of $\Theta(J)$, namely:

- $\Theta(J) = J-1$, which gives $\mathsf{k}(1) = 1$ (cf. (18));
- $\Theta(J) = \log J$, which gives $\mathsf{k}(1) = 0$;
- $\Theta(J) = \left(1-\frac{1}{J}\right)$, which gives $\mathsf{k}(1) = -1$.

From the discussion of Sect. 3.3, it should be clear that the three choices above induce potentially different effects on the stability range, as numerically detected by the mixed schemes. We also recall that, according to the results of [5] and [6] (cf.also Sect. 4.1), the numerical detected critical value is accurate when $\bar{\gamma}_{cr} \approx 6.60$.

• *Displacement-based schemes* Different order interpolations are used for triangular elements. The results are depicted in Table 1. We remark that, for this test, the stability range is accurately detected for all the schemes and all the choices for $\Theta(J)$. However, we notice that:

Table 2 Problem 1—Results for different functions $\Theta(J)$, triangular mixed elements

Elm	$\Theta(J)$	Mesh	$\bar{\gamma}_{cr}$ tension	Elm	$\Theta(J)$	Mesh	$\bar{\gamma}_{cr}$ tension
T2/T1	$(J-1)$	8×8	6.7	T2/P0	$(J-1)$	8×8	6.55
		16×16	6.60			16×16	6.6
		32×32	6.60			32×32	6.6
		64×64	6.60			64×64	6.6
	$\log J$	8×8	6.68		$\log J$	8×8	1.45
		16×16	6.65			16×16	1.07
		32×32	6.63			32×32	1.02
		64×64	6.60			64×64	1
	$(1-\frac{1}{J})$	8×8	6.68		$(1-\frac{1}{J})$	8×8	2.45
		16×16	6.63			16×16	0.575
		32×32	6.60			32×32	0.525
		64×64	6.60			64×64	0.525
T3/T2	$(J-1)$	4×4	6.68	MINI	$(J-1)$	8×8	7.425
		8×8	6.63			16×16	6.775
		16×16	6.60			32×32	6.675
		32×32	6.60			64×64	6.625
	$\log J$	4×4	6.63		$\log J$	8×8	1.25
		8×8	6.63			16×16	1.225
		16×16	6.60			32×32	1.15
		32×32	6.60			64×64	1.075
	$(1-\frac{1}{J})$	4×4	6.63		$(1-\frac{1}{J})$	8×8	0.625
		8×8	6.60			16×16	0.65
		16×16	6.60			32×32	0.625
		32×32	6.60			64×64	0.575

1. the condition number of the tangent matrix becomes significantly large with mesh refinement, especially for high-order schemes;
2. the use of low-order elements may give poor approximation results, due to the volumetric locking phenomenon.

• *Mixed schemes* Different mixed formulations were used to obtain results for the model problem. They are reported in Tables 2 and 3 (triangular and quadrilateral schemes, respectively).

We remark that the schemes, apart from the Taylor-Hood elements, are very sensitive to the choice of the function $\Theta(J)$. The best choice is here $\Theta(J) = J-1$. This should not be a surprise, because in this case the term (50) has a *stabilizing* effect, since we have $\hat{p}_h\,(\Theta''(1)+\Theta'(1)) = \gamma\, r_h \geq 0$ (r_h being an approximation of r, in most cases exactly coinciding with r). In addition, the worst choice is here $\Theta(J) = 1-1/J$.

We end this subsection by showing a couple of eigenvectors associated with the found numerical critical value. More precisely:

1. The eigenmode associated with the correct value $\bar{\gamma}_{cr} = 6.60$ for a solution using the T2/P1 element and $\Theta(J) = J-1$ (see Table 2) is depicted in Fig. 4. We remark that the computed eigenmode is physically reasonable. Here only the result for this element is plotted since the eigenmodes for other element formulations in Tables 1–3 leading to $\bar{\gamma}_{cr} \approx 6.60$ are very similar.
2. The eigenmode of the last converged state at $\bar{\gamma}_{cr} = 0.525$ is plotted in Fig. 5 for the T2/P0 element using the function $\Theta(J) = (1-\frac{1}{J})$, see Table 2. The local instability can be observed in the lower part of the domain. We remark that eigenmodes that are related to incorrect values $\bar{\gamma}_{cr} \neq 6.60$ can have different shapes. Usually one finds some local type of hourglassing or other unphysical instability.

6.1.2 Compression test

For the compression test, we explore the numerical behaviour only for a few elements and a single mesh, but we still consider all the three functions $\Theta(J)$ detailed in Sect. 6.1.1. We recall that, due to the results of [5] and [6], the numerical detected critical value is accurate when $\bar{\gamma}_{cr}$ approaches $-\infty$ (cf. (53)). From a computational point of view, we consider

Table 3 Problem 1—Results for different functions $\Theta(J)$, quadrilateral mixed elements

Elm	$\Theta(J)$	Mesh	$\bar{\gamma}_{cr}$ tension	Elm	$\Theta(J)$	Mesh	$\bar{\gamma}_{cr}$ tension
Q2/P1	$(J-1)$	8×8	6.6	Q1/P0	$(J-1)$	8×8	7.275
		16×16	6.6			16×16	6.775
		32×32	6.6			32×32	6.65
		64×64	6.6			64×64	
	$\log J$	8×8	1.325		$\log J$	8×8	2.375
		16×16	1.225			16×16	2.225
		32×32	1.125			32×32	1.9
		64×64	1.1			64×64	1.725
	$(1-\frac{1}{J})$	8×8	0.675		$(1-\frac{1}{J})$	8×8	1.625
		16×16	0.675			16×16	1.125
		32×32	0.575			32×32	0.95
		64×64	0.55			64×64	0.875

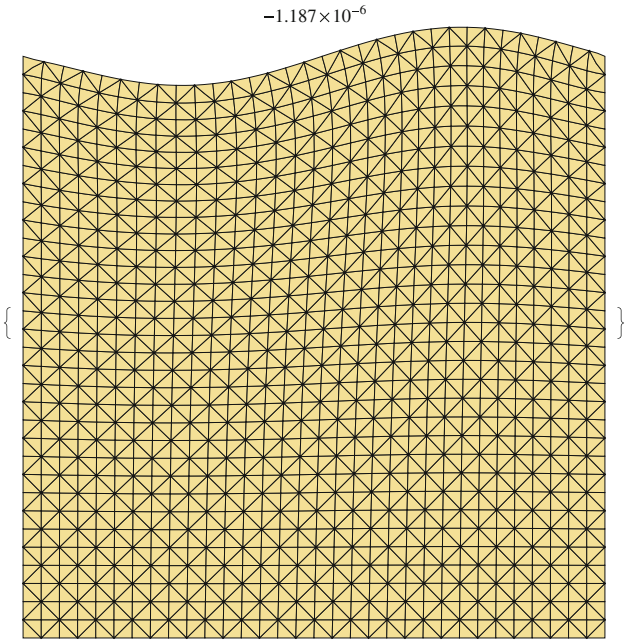

Fig. 4 Physical eigenmode at $\gamma = 6.60$ using the T2/P1 element and $\Theta(J) = J - 1$.

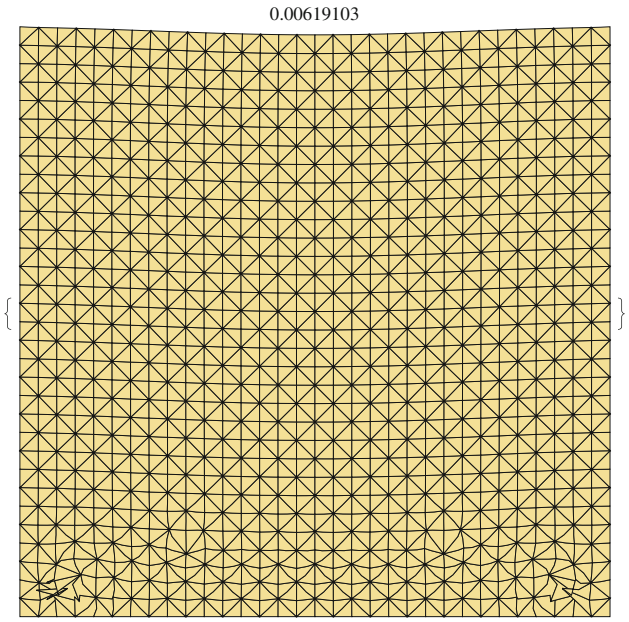

Fig. 5 Eigenmode of last converged solution at $\gamma = 0.525$ for T2/P0 and $\Theta(J) = (1 - \frac{1}{J})$.

the value $\bar{\gamma} = -660$ as the *numerical* $-\infty$. Accordingly, we stop our analysis at that value, if no eigenvalue sign change for the tangent matrix occurs before. The numerical results are reported in Table 4.

We remark that the mixed schemes are again sensitive to the choice of the function $\Theta(J)$. The best choice is here $\Theta(J) = 1 - 1/J$. Again, this should not be a surprise, because in this case the term (50) has a *stabilizing* effect, since we have $\hat{p}_h\ (\Theta''(1) + \Theta'(1)) = -\gamma\, r_h \geq 0$ (r_h being an approximation of r, in most cases exactly coinciding with r). Unfortunately, this optimal choice is the worst for the tension test. In addition, the worst choice for the compression test is the optimal one in the tension test.

6.2 Numerical results for Problem 2 (Sect. 4.2)

Also for this example we report the computed critical value $\bar{\gamma}_{cr}$. We recall that no results on the stability range is available for this problem (cf. Sect. 4.2).

• *Displacement-based schemes* In Table 5 we report the numerical results for displacement-based schemes on several meshes, and corresponding to $\Theta(J) = J - 1$.

Table 4 Problem 1—Results for different functions $\Theta(J)$, compression test

Elm	$\Theta(J)$	Mesh	$\bar{\gamma}_{cr}$ compression
T4	$(J-1)$	16×16	$-660\,(-\infty)$
	$\log J$	16×16	$-660\,(-\infty)$
	$(1-1/J)$	16×16	$-660\,(-\infty)$
T2/T1	$(J-1)$	32×32	-535
	$\log J$	32×32	$-660\,(-\infty)$
	$(1-1/J)$	32×32	$-660\,(-\infty)$
T2/P0	$(J-1)$	32×32	-77.5
	$\log J$	32×32	-100
	$(1-1/J)$	32×32	-125

Table 5 Problem 2—Results for $\Theta(J)=J-1$, displacement-based elements

Elm	$\Theta(J)$	Mesh	$\bar{\gamma}_{cr}$
T4	$(J-1)$	4×2	90.4
		8×4	75.5
		16×8	71.6
		32×16	65.1
		64×32	62.3
T3	$(J-1)$	16×8	96.9
		32×16	78.41
		64×32	69.54
		128×64	63.18
T2	$(J-1)$	16×8	80.8
		32×16	71.8
		64×32	67.3
		128×64	64.2
		256×128	62.2

Table 6 Problem 2—Results for $\Theta(J)=J-1$, triangular mixed elements

Elm	$\Theta(J)$	Mesh	$\bar{\gamma}_{cr}$
MINI	$(J-1)$	32×16	86.0
		32×64	74.7
		64×128	68.2
		128×256	64.5
T2/P0	$(J-1)$	16×8	58.0
		32×16	53.6
		64×32	58.9
		128×64	57.7
T2/T1	$(J-1)$	16×8	53.3
		32×16	62.5
		64×32	62.6
		128×64	62.9
T3/T2	$(J-1)$	16×8	70.7
		32×16	64.7
		64×32	62.3
		128×64	61.2

Table 7 Problem 2—Results for $\Theta(J)=J-1$, quadrilateral mixed elements

Elm	$\Theta(J)$	Mesh	$\bar{\gamma}_{cr}$
Q2/P1	$(J-1)$	16×8	60.5748
		32×16	57.3658
		64×32	55.2208
		128×64	40.128
Q1/P0	$(J-1)$	32×16	69.0
		64×32	64.7
		128×64	62.6
		256×128	61.6

• *Mixed schemes* Still for the choice $\Theta(J)=J-1$, we report the numerical results for several mixed schemes and meshes in Tables 6 and 7 (triangular and quadrilateral elements, respectively).

• *Different Choices of* $\Theta(J)$ We now consider a selection of finite element schemes. For each element we fix a representative mesh, in such a way that the corresponding degrees of freedom are comparable. We then investigate on the numerical behaviour in detecting the stability range for the three functions $\Theta(J)$ presented in Sect. 6.1.1 (Table 8).

7 Conclusions

In this paper we have considered several finite element schemes for the approximation of large deformation elastic problems in the nearly incompressible and purely incompressible regimes. In particular, we focused on the method's ability to accurately reproduce the stability range of a given problem, i.e. the ability to accurately capture critical loads for the possible occurrence of bifurcation and limit points. By means of a couple of 2D model problems involving a very simple neo-Hookean constitutive law, we were able to highlight the following issues.

Concerning the *displacement/pressure* mixed formulation:

- Even finite element schemes which are known to perform optimally in the infinitesimal framework, may fail the stability range detection to large extent. This is the case of the MINI element and the popular Q2/P1 element, for instance. For the MINI element, a rigorous (though not optimal) analysis of the failure to detect the stability range for Problem 1 (Sect. 4.1), and with $\Theta(J)=\ln J$, has been developed in [5].

Table 8 Problem 2—Results for different functions $\Theta(J)$

Elm	$\Theta(J)$	Mesh	$\bar{\gamma}_{cr}$
T4	$(J-1)$	32×16	59.328
	$\log J$	32×16	59.328
	$(1-1/J)$	32×16	59.328
T2/T1	$(J-1)$	64×32	62.5753
	$\log J$	64×32	64.6257
	$(1-1/J)$	64×32	65.3834
T2/P0	$(J-1)$	64×32	50.265
	$\log J$	64×32	62.703
	$(1-1/J)$	64×32	62.230

- The discrete stability range, as numerically detected, depends on both the scheme and on the function $\Theta(J)$ which models the volumetric term in the elastic energy density. For the incompressible limit situation, the more the numerical scheme relaxes the incompressibility constraint, the more the discrete stability range tends to be inaccurately approximated.

For the *displacement-based* formulation:

- In the nearly incompressible regime, the methods seem to be robust in detecting the stability range. However, we notice that, in order to avoid volumetric locking effect, high-order elements should be preferred. This implies very large condition numbers for the resulting tangent matrices.

Possible promising alternatives for an accurate approximation of large deformation elastic problems are as follows.

1. The use of *NURBS-based* approximation schemes. On the one hand, the higher inter-element continuity might alleviate the ill-conditioning effects when dealing with the *displacement-based* formulation. Even though in a different context, some numerical evidence of this possible improvement in the condition number of the stiffness matrix can be found in [9]. On the other hand, the exact satisfaction of the incompressibility constraint seems to be accessible when dealing with the *displacement/pressure* mixed formulation or even with a higher-order formulation involving a stream function (see [6] and [7] for first attempts towards this direction).
2. The use of different mixed formulation. For instance, one may think of considering the Hu-Washizu formulation as the basis for the discretization procedure. We report promising results obtained following this strategy: Table 9 displays the outcomes concerning the problem of Sect. 6.1.1, while Table 10 those concerning the problem of Sect. 6.2. For details on the employed approximation scheme, we refer to [23].

Table 9 Problem 1—Results for different functions $\Theta(J)$, Hu-Washizu mixed element

Elm	$\Theta(J)$	Mesh	$\bar{\gamma}_{cr}$ tension
Q1/EI4	$(J-1)$	8×8	7.5
		16×16	6.85
		32×32	6.675
		64×64	6.625
	$\log J$	8×8	7.5
		16×16	6.85
		32×32	6.675
		64×64	6.625
	$(1-\frac{1}{J})$	8×8	7.5
		16×16	6.85
		32×32	6.675
		64×64	6.625

Table 10 Problem 2—Results for $\Theta(J) = J - 1$, Hu-Washizu mixed element

Elm	$\Theta(J)$	Mesh	$\bar{\gamma}_{cr}$
Q1/EI4	$(J-1)$	32×16	78.8
		64×32	70.0
		128×64	65.5
		256×128	63.1

Other possible techniques to explore are the ones taking advantage of *Discontinuous Galerkin* or *nonconforming* approaches.

We finally remark that an exhaustive theoretical analysis about the method capability to capture the stability range for a general large deformation elastic problem is still missing.

Acknowledgments The authors were partially supported by the European Commission through the FP7 Factory of the Future project *TERRIFIC* (FoF-ICT-2011.7.4, Reference: 284981), by the European Research Council through the FP7 Ideas Starting Grants n. 259229 *ISOBIO* and n. 205004 *GeoPDEs*, as well as by the Italian MIUR through the FIRB "Futuro in Ricerca" Grant RBFR08CZ0S and through the PRIN Project n. 2010BFXRHS. These supports are gratefully acknowledged.

References

1. AceFEM© webpage. http://www.wolfram.com/products/applications/acefem/
2. AceGen© webpage. http://www.wolfram.com/products/applications/acegen/
3. Arnold DN, Brezzi F, Fortin M (1984) A stable finite element for the Stokes equation. Calcolo 21:337–344
4. Auricchio F, Brezzi F, Lovadina C (2004) Mixed finite element methods, chap. 9. In: Stein E, De Borst R, Hughes TJR (eds) Encyclopedia of computational mechanics, vol 1. Wiley, Philadelphia

5. Auricchio F, Beirão da Veiga L, Lovadina C, Reali A (2005) A stability study of some mixed finite elements for large deformation elasticity problems. Comput Methods Appl Mech Eng 194:1075–1092
6. Auricchio F, Beirão da Veiga L, Lovadina C, Reali A (2010) The importance of the exact satisfaction of the incompressibility constraint in nonlinear elasticity: mixed FEMs versus NURBS-based approximations. Comput Methods Appl Mech Eng 199:314–323
7. Auricchio F, Beirão da Veiga L, Buffa A, Lovadina C, Reali A, Sangalli G (2007) A fully "locking-free" isogeometric approach for plane linear elasticity problems: a stream function formulation. Comput Methods Appl Mech Eng 197:160–172
8. Bazilevs Y, Beirão de Veiga L, Cottrell JA, Hughes TJR, Sangalli G (2006) Isogeometric analysis: approximation, stability and error estimates for *h*-refined meshes. Math Models Methods Appl Sci 16:1–60
9. Beirão da Veiga L, Cho D, Pavarino LF, Scacchi S (2012) Overlapping Schwarz methods for isogeometric analysis. SIAM J Numer Anal 50:1394–1416
10. Bonet J, Wood RD (1997) Nonlinear continuum mechanics for finite element analysis. Cambridge University Press, Cambridge
11. Braess D, Ming P (2005) A finite element method for nearly incompressible elasticity problems. Math Comp 74:2552
12. Brezzi F, Fortin M (1991) Mixed and hybrid finite element methods. Springer-Verlag, New York
13. Carstensen C, Dolzmann G (2004) An a priori error estimate for finite element discretizations in nonlinear elasticity for polyconvex materials under small loads. Numer Math 97:67–80
14. Ciarlet PG (1998) Mathematical elasticity. vol 1: three dimensional elasticity. Elsevier, North-Holland
15. Dobrowolski M (1992) A mixed finite element method for approximating incompressible materials. SIAM J Numer Anal 29:365–389
16. Gurtin ME (1981) An introduction to continuum mechanics. Academic Press, New York
17. Hughes TJR (2000) The finite element method. Dover Publications, New York
18. Hughes TJR, Cottrell JA, Bazilevs Y (2005) Isogeometric analysis: CAD, finite elements, NURBS, exact geometry, and mesh refinement. Comput Methods Appl Mech Eng 194:4135–4195
19. Le Tallec P (1994) Numerical methods for nonlinear three-dimensional elasticity. In: Ciarlet PG, Lions JL (eds) Handbook of numerical analysis, vol 3. Elsevier, North-Holland, pp 465–622
20. Lovadina C, Auricchio F (2003) On the enhanced strain technique for elasticity problems. Comput Struct 81:777–787
21. Malvern LE (1969) Introduction to the mechanics of a continuous medium. Prentice-Hall, Englewood Cliffs
22. Marsden JE, Hughes TJR (1993) Mathematical foundations of elasticity. Dover Publications, New York
23. Mueller-Hoeppe DS, Loehnert S, Wriggers P (2009) A finite deformation brick element with inhomogeneous mode enhancement. Int J Numer Methods Eng 78:1164–1187
24. Ogden RW (1997) Non-linear elastic deformations. Dover Publications, New York
25. Pantuso D, Bathe KJ (1997) On the stability of mixed finite elements in large strain analysis of incompressible solids. Finite Elem Anal Des 28:83–104
26. Ruas V (1989) Existence and stability of asymmetric finite-element approximations in nonlinear incompressible analysis. SIAM J Numer Anal 26:1031–1059
27. Wriggers P, Reese S (1996) A note on enhanced strain methods for large deformations. Comput Methods Appl Mech Eng 135:201–209
28. Yamada T, Kikuchi F (1990) A mixed finite element method for large deformation analysis of incompressible hyperelastic materials. Theor Appl Mech 39:61–73
29. Yamada T, Kikuchi F (1993) An arbitrary Lagrangian-Eulerian finite element method for incompressible hyperelasticity. Comput Meth Appl Mech Eng 102:149–177